IBBUL
Lapai Journal of Applied and Natural Sciences
LAJANS Vol 10(3s): 285-292

RESEARCH PAPER

A Laplace Transform Approach to Gaussian Plume Modelling of Atmospheric Carbon Dioxide Dispersion

***[1]Ogbada, N., [2]Jimoh, O.R., & [2]Salihu, N.O.**

[1]*Department of Mathematics and Statistics, Federal University of Technology, Ikot Abasi, Nigeria*
[2]*Department of Mathematics, Federal University of Technology, Minna, Nigeria*

ABSTRACT

This paper presents a modified Laplace transform approach to analysing the atmospheric dispersion of carbon dioxide (CO_2), using the Ibom Power Thermal Plant as a case study. The adaptation of the Gaussian plume model for CO_2 dispersion from Nigerian thermal power plants remains limited. This work addresses this gap by developing a localized model that integrates site-specific emission and meteorological data to predict spatial CO_2 concentration fields under steady-state conditions. The governing advection–diffusion equation was solved analytically using Laplace transform and implemented in Maple for simulation and visualization. Model parameters, including emission rate, wind velocity, and atmospheric stability classes, were estimated from Ibom Power operational data and Norwegian Meteorological Institute datasets. Results revealed that CO_2 concentration impacts ground-level air quality most significantly between 2500 m and 3500 m downwind, after which it decreases exponentially with distance. The novelty of this work lies in its site-specific adaptation of the Gaussian plume model to Nigeria's humid coastal environment and its inclusion of a reaction term in the standard Gaussian model equation. The findings from this research provide valuable insights to land planners on situating sensitive receptors such as schools, hospitals, and residential areas away from high-exposure zones.

Keywords: Gaussian plume model, Atmospheric dispersion, Pollutant modelling, Laplace transform method

INTRODUCTION

According to the Intergovernmental Panel on Climate Change (IPCC, 2021), energy is responsible for about 73% of all CO_2 emissions worldwide. The International Energy Agency (IEA) also claims that transportation, industrial activity and thermal power plant combustion of fossil fuels mostly cause these emissions (IEA, 2022). Our case study, the Ibom Power Plant, is a 191 megawatts (MW) gas-fired facility situated in Ikot Abasi, Akwa Ibom State, Nigeria, is one of many facilities where fast energy demand is matched by rising environmental concerns. Modelling the dispersion of CO_2 from point sources like thermal power plants is vital for environmental impact assessment and strategic urban planning. Among the most established tools for this purpose is the Gaussian plume model, which provides a mathematical representation of pollutant dispersion in the atmospheric boundary layer under steady-state conditions (Seinfeld and Pandis, 2016). This model has been widely adopted due to its computational simplicity and ability to approximate real-world scenarios when supplied with appropriate meteorological and emissions data. In the specific context of Ibom Power Plant, the Gaussian plume model is particularly appropriate because it assumes continuous emissions and steady-state atmospheric conditions, assumptions that align closely with the plant's operational profile. The methodology outlined in this study builds on the standard analytical solution to the species transport

Received 25 October, 2025
Accepted 30 December, 2025
Address Correspondence to: nathanielogbada@gmail.com; *Tel. +234 8106287010*

equation, simplifying it through assumptions such as steady state and constant wind profiles. These are commonly accepted in preliminary atmospheric modelling studies (Zhang et al., 2021).

Thermal power plants are stationary sources of atmospheric carbon dioxide (CO_2) emissions due to their dependence on fossil fuel combustion for electricity generation. Unlike mobile sources such as vehicles, which emit pollutants along transit routes, power plants discharge pollutants from fixed locations, typically via elevated stacks. This makes them ideal for point-source pollution modelling. Among the various greenhouse gases emitted, CO_2 is the most prevalent, and its contribution to global warming and climate change is well documented (IEA, 2023). Natural gas, which powers several plants in Nigeria, emits significantly less CO_2 than coal or oil per unit of energy produced. However, gas-fired plants still contribute substantially to total greenhouse gas emissions, particularly in developing countries lacking carbon capture and storage (CCS) technologies (United States Environmental Protection Agency, 2025).

In sub-Saharan Africa, the overall contribution to global emissions remains low (approximately 3%–4%), yet emissions have grown rapidly in recent years due to population growth, industrialization and increased deployment of thermal power plants (IEA, 2019). Nigeria, in particular, is a regional leader in fossil fuel power generation, and its power sector emissions are projected to grow in the absence of large-scale transitions to renewable energy (Awodumi and Adewuyi, 2020). A study in Nigeria examining data from 1990 to 2020 found a feedback relationship between Foreign Direct Investment (FDI) inflows and CO_2 emissions, as well as a unidirectional causal relationship from economic growth to emissions. This suggests that both FDI and economic growth contribute to increased CO_2 emissions in the country (Ogunjobi et al., 2024).

Understanding the dispersion characteristics of CO_2 is crucial, especially concerning potential leaks from CCS infrastructure. A study utilized computational fluid dynamics (CFD) to investigate CO_2 dispersion from high-pressure pipelines over complex terrain. The research highlighted that CO_2, being denser than air, tends to accumulate at ground level, posing asphyxiation risks. The study also noted that the Joule-Thomson effect causes a sharp temperature drop during CO_2 release, influencing its dispersion behavior (Wang et al., 2021). Another study employed CFD analysis to simulate CO_2 dispersion dynamics in confined spaces, such as industrial settings. The findings emphasized that can accumulate rapidly in enclosed areas, reaching lethal concentrations above 12% by volume. This underscores the importance of effective ventilation and monitoring systems to protect people from CO_2 exposure (Cioclea et al., 2024).

To address CO_2 emissions, Carbon Capture, Utilization and Storage (CCUS) technologies have gained prominence. The International Energy Agency's (IEA, 2020) report highlighted CCUS as essential for reducing emissions in key sectors and for removing CO_2 to achieve net-zero goals. The report identified four key contributions of CCUS: tackling emissions from existing energy infrastructure, providing solutions for sectors with hard-to-abate emissions, serving as a platform for low-carbon hydrogen production and removing CO_2 from the atmosphere (IEA, 2020). The Ibom Power Plant case study is particularly relevant due to its geographic and operational features, namely: its central role in Nigeria’s electricity generation and its proximity to residential areas.

The model implementation in this study leverages Maple software to visualize dispersion patterns. This reflects a growing trend in environmental modelling, where open-source tools are increasingly used for simulation and visualization due to their accessibility and flexibility (Samborska-Goik and Pogrzeba, 2024).

METHODOLOGY

The dispersion of CO_2 in the atmosphere is governed by the species transport equation given by:

$$\frac{\partial(C)}{\partial t} + U\frac{\partial C}{\partial x} = D_x\frac{\partial^2 C}{\partial x^2} + D_y\frac{\partial^2 C}{\partial y^2} + D_z\frac{\partial^2 C}{\partial z^2} + S(x,y,z) - k_r C \quad (1)$$

Where C is the concentration of CO_2 at location (x,y,z), U is the mean speed in x–directions, D_x, D_y, D_z are the diffusion coefficients in the x, y and z directions, $S(x,y,z)$ is the source term for CO_2 emissions and k_r is the reaction term for CO_2.

The following initial and boundary conditions were applied to reflect realistic atmospheric dispersion of CO_2.

Initial condition:

i. The initial pollutant concentration of CO_2 is zero. It is represented as: $C(x,y,z,0) = 0$.

Boundary conditions:

i. **Source condition:** The pollutant is emitted

continuously at a constant rate Q from a point source located at $(x,y,z) = (0,0,H_e)$.
At $x = 0$, emission rate $= Q[g/s]$. This source condition is incorporated via a Dirac delta function $\delta(y)\delta(z-H_e)$ in the governing equation to model a point source at height H. This is expressed mathematically as:

$$uC|_{x=0} = Q\delta(y)\delta(z-H_e)$$

ii. **Ground boundary (reflecting ground at $z = 0$ for all x and y):** No flux through the ground, that is, a perfect reflection occurs (assuming the pollutant does not deposit or get absorbed). This is mathematically expressed as:

$$\left.\frac{\partial C}{\partial z}\right|_{z=0} = 0$$

At $z = 0$, the solution is constructed as the sum of two plumes, that is:

$$\mathrm{C(x,y,z)} = \mathrm{C_{real}(x,y,z)} + \mathrm{C_{image}(x,y,z)}$$

The spatial dispersion of CO_2 emissions is modelled from point sources in an energy system under steady atmospheric conditions as stated below:

Mathematical assumptions

To simplify the problem, the following assumptions were made:

i. No pollutant was present in the atmosphere before the source began emitting CO_2.
ii. The system maintains a steady state, that is $\frac{\partial C}{\partial t} = 0$.
iii. The wind speed is high enough that advection dominates diffusion in the x–direction which implies that $D_x \approx 0$.
iv. The speed of the wind U, is constant in the x–direction.
v. The terrain is flat and has an infinite domain.

Considering the above assumptions, equation (1) is reduced to a parabolic Partial Differential Equation (PDE) as thus:

$$U\frac{\partial C}{\partial x} = D_y\frac{\partial^2 C}{\partial y^2} + D_z\frac{\partial^2 C}{\partial z^2} + S(x,y,z) - k_r C \quad (2)$$

As discussed in Atmospheric Chemistry and Physics by Seinfeld and Pandis (2016), the source term in the advection-diffusion equation is expressed as $S(x,y,z) = \frac{Q}{U}\delta(x)\delta(y)\delta(z-H_e)$, where H_e is the effective stack height. This follows that equation (2) can be re-written after applying the source boundary condition as:

$$U\frac{\partial C}{\partial x} = D_y\frac{\partial^2 C}{\partial y^2} + D_z\frac{\partial^2 C}{\partial z^2} + \frac{Q}{U}\delta(y)\delta(z-H_e) - k_r C \quad (3)$$

Analytical solution

To solve the steady-state advection–diffusion equation, the Laplace transform technique is applied in the downwind direction (x), treating it as a pseudo-time variable due to advection dominance. Solving equation (3) using Laplace transform in the x–direction, we define the Laplace transform of $\mathrm{C}(x,y,z)$ as:

$$L\{\mathrm{C}(x,y,z)\} = \tilde{C}(s,y,z) = \int_0^\infty C(x,y,z)e^{-sx}dx \quad (4)$$

Equation (3) is a parabolic PDE with x acting like time, we therefore treat x as a "psuedo-time" and apply the Laplace transform with respect to x as thus:

$$\mathrm{L}\left\{U\frac{\partial C}{\partial x}\right\} = \mathrm{L}\left[D_y\frac{\partial^2 C}{\partial y^2} + D_z\frac{\partial^2 C}{\partial z^2} + \frac{Q}{U}\delta(y)\delta(z - H_e) - k_r C\right] \quad (5)$$

$$U\left[s\tilde{C}(s,y,z) - C(x,y,z,0)\right] = L\left\{D_y\frac{\partial^2 C}{\partial y^2}\right\} + L\left\{D_z\frac{\partial^2 C}{\partial z^2}\right\} + L\left\{\frac{Q}{U}\delta(y)\delta(z - H_e)\right\} + L\{k_r C\} \quad (6)$$

Performing a Laplace transform of equation (5) and applying the initial concentration condition $C(x,y,z,0) = 0$, we have:

$$U\left[s\tilde{C}(s,y,z)\right] = D_y\frac{\partial^2\tilde{C}}{\partial y^2} + D_z\frac{\partial^2\tilde{C}}{\partial z^2} + \frac{Q}{U}\delta(y)\delta(z - H_e) - k_r\tilde{C} \quad (7)$$

Rearranging equation (7) into Helmholtz form, we have:

$$D_y\frac{\partial^2\tilde{C}}{\partial y^2} + D_z\frac{\partial^2\tilde{C}}{\partial z^2} - [\mathrm{Us} + k_r]\tilde{C}(s,y,z) = -\frac{Q}{U}\delta(y)\delta(z - H_e) \quad (8)$$

The proper scaling of equation (8) comes from making the equation isotropic. Stretched coordinates are introduced to normalize diffusion effects so that D_y and D_z no longer appear explicitly in equation (8) as thus:

$$\text{Let } y' = \frac{y}{\sqrt{D_y}} \text{ and } z' = \frac{z}{\sqrt{D_z}} \quad (9)$$

The derivatives in equation (8) are transformed thus:

$$\left.\begin{aligned} \frac{\partial\tilde{C}}{\partial y} &= \frac{\partial\tilde{C}}{\partial y'}\cdot\frac{\partial y'}{\partial y} = \frac{1}{\sqrt{D_y}}\frac{\partial\tilde{C}}{\partial y'} \\ \frac{\partial\tilde{C}}{\partial z} &= \frac{\partial\tilde{C}}{\partial z'}\cdot\frac{\partial z'}{\partial z} = \frac{1}{\sqrt{D_z}}\frac{\partial\tilde{C}}{\partial z'} \end{aligned}\right\} \quad (10a)$$

Similarly,

$$\left.\begin{aligned} \frac{\partial^2\tilde{C}}{\partial y^2} &= \frac{1}{D_y}\frac{\partial^2\tilde{C}}{\partial y'^2} \\ \frac{\partial^2\tilde{C}}{\partial z^2} &= \frac{1}{D_z}\frac{\partial^2\tilde{C}}{\partial z'^2} \end{aligned}\right\} \quad (10b)$$

By substituting equation (10b) back into equation (8),

$$D_y\left(\frac{1}{D_y}\frac{\partial^2\tilde{C}}{\partial y'^2}\right) + D_z\left(\frac{1}{D_z}\frac{\partial^2\tilde{C}}{\partial z'^2}\right) - [\mathrm{Us} + k_r]\tilde{C}(s,y,z) = -\frac{Q}{U}\delta(y)\delta(z - H_e) \quad (11)$$

Equation (11) simplifies to:

$$\frac{\partial^2\tilde{C}}{\partial y'^2} + \frac{\partial^2\tilde{C}}{\partial z'^2} - [\mathrm{Us} + k_r]\tilde{C}(s,y,z) = -\frac{Q}{U}\delta(y)\delta(z - H_e) \quad (12)$$

The following new coordinates are introduced to simplify equation (12):

$$\text{Let } \delta(y') = \delta(y)\sqrt{D_y} \text{ and } \delta(z') = \delta(z - H_e)\sqrt{D_z} \quad (13a)$$

$$\text{That is, } \delta(y) = \frac{1}{\sqrt{D_y}}\delta(y') \text{ and } \delta(z - H_e) = \frac{1}{\sqrt{D_z}}\delta(z') \quad (13b)$$

Substituting equation (13b) into the delta function in equation (12), the following equation was obtained:

$$\frac{\partial^2\tilde{C}}{\partial y'^2} + \frac{\partial^2\tilde{C}}{\partial z'^2} - [\mathrm{Us} + k_r]\tilde{C}(s,y,z) = -\frac{Q}{U}\frac{1}{\sqrt{D_y}}\delta(y')\frac{1}{\sqrt{D_z}}\delta(z') \quad (14)$$

That is;

$$\frac{\partial^2\tilde{C}}{\partial y'^2} + \frac{\partial^2\tilde{C}}{\partial z'^2} - [\mathrm{Us} + k_r]\tilde{C}(s,y,z) = -\frac{Q}{U\sqrt{D_y D_z}}\delta(y')\delta(z') \quad (15)$$

Equation (15) gives the final transformed isotropic equation in 2D space and it is of the form:

$$\nabla^2\tilde{C} - \lambda^2\tilde{C} = -A\delta(y')\delta(z') \quad (16)$$

Where: $\lambda^2 = [\mathrm{Us} + k_r\,]$ and $A = \frac{Q}{U\sqrt{D_yD_z}}$

Equation (16) is a standard 2D Helmholtz equation, which can be solved using the Green's function for 2D space.

The Green's function for the 2D modified Helmholtz equation is given by:

$$\nabla^2 G(\vec{r}) - \lambda^2 G(\vec{r}) = -\delta(\vec{r}) \quad (17)$$

And the standard solution for the Green's function is given by:

$$G(\vec{r}) = \frac{1}{2\pi}k_0(\lambda|\vec{r}|)$$

Where: k_0 is the modified Bessel function of the second kind, order zero

and $|\vec{r}| = \sqrt{y^2 + (z-H)^2}$ is the distance from the source point.

Comparing equations (16) and (17), the solution for equation (16) therefore becomes:

$$\tilde{C}(s,y',z') = \frac{1}{2\pi}Ak_0\left(\lambda\sqrt{y^2 + (z-H)^2}\right) \quad 18)$$

Recall that $\lambda^2 = [\mathrm{Us} + k_r\,]$ and $\mathrm{A} = \frac{Q}{U\sqrt{D_yD_z}}$. Substituting into equation (18) we have:

$$\tilde{C}(s,y',z') = \frac{\mathrm{Q}}{2\pi\mathrm{U}\sqrt{D_yD_z}}k_0\left(\sqrt{[\mathrm{Us} + k_r\,]}\sqrt{\frac{y^2}{\mathrm{D_y}} + \frac{(\mathrm{z}-H_e)^2}{\mathrm{D_z}}}\right) \quad (19)$$

By finding the inverse Laplace transform of equation (19), the Gaussian solution is obtained as follows;

$$\tilde{C}(s,y',z') = \frac{\mathrm{Q}}{2\pi\mathrm{U}\sqrt{D_yD_z}}k_0\left(\sqrt{[\mathrm{Us} + k_r\,]}\cdot k\right) \quad (20)$$

Where $k = \sqrt{\frac{y^2}{D_y} + \frac{(z-H_e)^2}{D_z}}$

Let $b = Us$ and $\alpha = k_r$ in equation (20). Therefore, equation (20) further reduces to:

$$\tilde{C}(s,y',z') = \frac{\mathrm{Q}}{2\pi\mathrm{U}\sqrt{D_yD_z}}k_0\left(k\sqrt{b+\alpha}\right) \quad (21)$$

From Laplace transform table,

$$L^{-1}\left\{k_0\left(k\sqrt{b+\alpha}\right)\right\} = \frac{1}{2t}exp\left(-\alpha t - \frac{k^2}{4t}\right)$$

Now, performing an inverse Laplace transform of the entire equation (21) we have;

$$L^{-1}\left\{\tilde{C}(s,y',z')\right\} = L^{-1}\left\{\frac{\mathrm{Q}}{2\pi\mathrm{U}\sqrt{D_yD_z}}\right\}\cdot L^{-1}\left\{k_0\left(k\sqrt{b+\alpha}\right)\right\} \quad (22)$$

$$\Longrightarrow \mathrm{C(x,y,z)} = \frac{\mathrm{Q}}{2\pi\mathrm{U}\sqrt{D_yD_z}}\cdot\frac{1}{2t}exp\left(-\alpha t - \frac{k^2}{4t}\right) \quad (23)$$

From the definition of velocity $V = \frac{x}{t}$, we have $t = \frac{x}{U}$. Substituting for t in equation (23) gives:

$$\mathrm{C(x,y,z)} = \frac{\mathrm{Q}}{2\pi\mathrm{U}\sqrt{D_yD_z}}\cdot\frac{U}{2x}exp\left(-\alpha\frac{x}{U} - \frac{Uk^2}{4x}\right) \quad (24)$$

Recall that $k^2 = \frac{y^2}{D_y} + \frac{(z-H_e)^2}{D_z}$ and $\alpha = k_r$, substituting into equation (24), we have:

$$\mathrm{C(x,y,z)} = \frac{\mathrm{Q}}{4\pi x\sqrt{D_yD_z}}exp\left(-k_r\frac{x}{U} - \frac{U}{4x}\left(\frac{y^2}{D_y} + \frac{(z-H_e)^2}{D_z}\right)\right) \quad (25)$$

We define the dispersion coefficients as:

$$\sigma_y^2 = 2D_y\frac{x}{U} \text{ and } \sigma_z^2 = 2D_z\frac{x}{U}$$

Therefore, $D_y = \frac{\sigma_y^2 U}{2x}$ and $D_z = \frac{\sigma_z^2 U}{2x}$. By substituting the values of D_y and D_z into equation (25),

$$\mathrm{C(x,y,z)} = \frac{\mathrm{Q}}{4\pi x\sqrt{\frac{\sigma_y^2 U}{2x}\frac{\sigma_z^2 U}{2x}}}\, exp\left(-k_r\frac{x}{U} - \frac{U}{4x}\left(\frac{y^2}{\frac{\sigma_y^2 U}{2x}} + \frac{(z-H_e)^2}{\frac{\sigma_z^2 U}{2x}}\right)\right) \quad (26)$$

Simplifying equation (26), we have:

$$\mathrm{C(x,y,z)} = \frac{\mathrm{Q}}{2\pi U\sigma_y\sigma_z}\, exp\left(-\frac{y^2}{2\sigma_y^2} - k_r\frac{x}{U} - \frac{(z-H_e)^2}{2\sigma_z^2}\right) \quad (27)$$

We apply the final boundary condition as thus:

The result is an image source method where an imaginary source is placed at $\mathrm{z} = -H_e$ to satisfy the reflection symmetry below. This is done to model reflection from the ground and inversion layers, ensuring no flux through boundaries.

$$\mathrm{C(x,y,z)} = \mathrm{C_{real}(x,y,z)} + \mathrm{C_{image}(x,y,z)}$$

Equation (27) therefore becomes:

$$\mathrm{C(x,y,z)} = \frac{Q}{2\pi U\sigma_y\sigma_z}\, exp\left(-\frac{y^2}{2\sigma_y^2} - k_r\frac{x}{U} - \frac{(z-H_e)^2}{2\sigma_z^2}\right) + \frac{Q}{2\pi U\sigma_y\sigma_z}\, exp\left(-\frac{y^2}{2\sigma_y^2} - k_r\frac{x}{U} - \frac{(z+H_e)^2}{2\sigma_z^2}\right) \quad (28)$$

Equation (28) can be reduced to:

$$\mathrm{C(x,y,z)} = \frac{Q}{2\pi U\sigma_y\sigma_z}\exp\left(-\frac{y^2}{2\sigma_y^2} - k_r\frac{x}{U}\right)\left[exp\left(-\frac{(z-H_e)^2}{2\sigma_z^2}\right) + exp\left(-\frac{(z+H_e)^2}{2\sigma_z^2}\right)\right] \quad (29)$$

The equation (29) above is the approximate collocation solution for the concentration of CO_2 in the atmosphere at any spatial location incorporating a first-order reaction term.

RESULTS AND DISCUSSION

Figures 1 – 4 below were obtained from the analytical solution in equation (29) with the aid of MAPLE 2023.0 software.

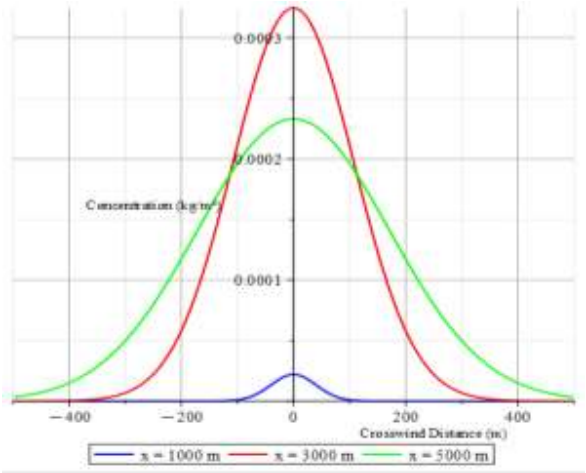

Fig. 1: Graph of Crosswind Concentration Profile at $x = 1000$, $x = 2000$ and $x = 5000$. The parameters used are: $Q = 30.61\mathrm{kg/s}$, $U = 3\ m/s$, $H_e = 50\ m$, $k_r = 0.00001\ 1/m$ and the dispersion coefficients $\sigma_y(x)$ and $\sigma_z(x)$ used are for stability class-D (neutral) as captured on the Pasquill-Gifford table (Turner, 1994).

Figure 1 shows how CO_2 spreads out sideways from the power plant when measured at 1000m, 2000m and 5000m away at ground level. The highest concentration is found right in the middle, directly in line with the wind coming from the stack and it increases with an increase in distance. It therefore implies that people, vegetation, or sensors located directly downwind will experience much higher CO_2 exposure.

Figure 2 compares how CO_2 spreads out vertically in the air 500 m,1000 m and 3000 m away from the power plant, right under the

middle of the plume. The highest CO_2 is found about 50 meters above the ground for all the distances, which is roughly how high the plume is after it rises from the stack. Above and below this height, the CO_2 drops off quickly.

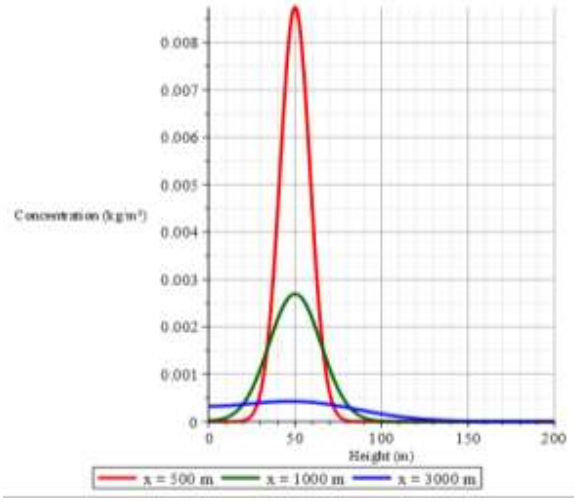

Fig. 2: Graph of Vertical Concentration Profile at $x = 500$, $x = 1000$ and $x = 3000$.

At ground level, there's almost no CO_2 because the plume is still floating high in the air. This implies that close to the plant; the pollution mostly affects the air up high and it only starts mixing down to the ground further away as captured at 3000m away from the power plant.

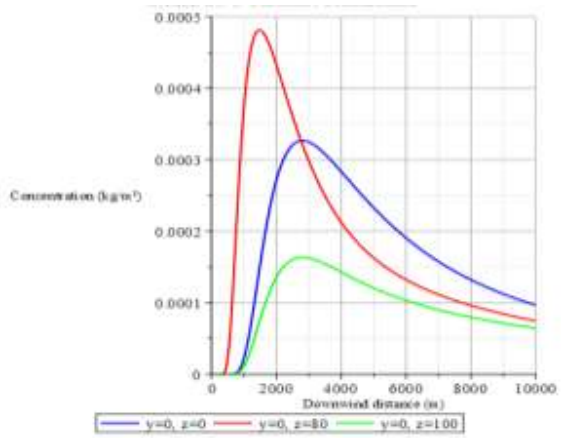

Fig. 3: Graph of Ground-Level Concentration Profile at $z = 0$, $z = 80$ and $z = 100$.

Figure 3 captures the ground-level concentration profile at 0m, 80m and 100m above ground level. It shows that CO_2 concentration initially increases with downwind distance, reaching a maximum value of approximately 0.00031 kg/m³ and 0.00016 kg/m³ at around 3000 m from the stack for both 0m and 100m respectively above ground level. It is observed that at 80 m above ground level, the peak concentration is approximately 0.00048 kg/m³ at around 1500 m from the stack due to its closeness to the stack height of 50m. Beyond the peak points, the concentration decreases steadily as the plume continues to disperse.

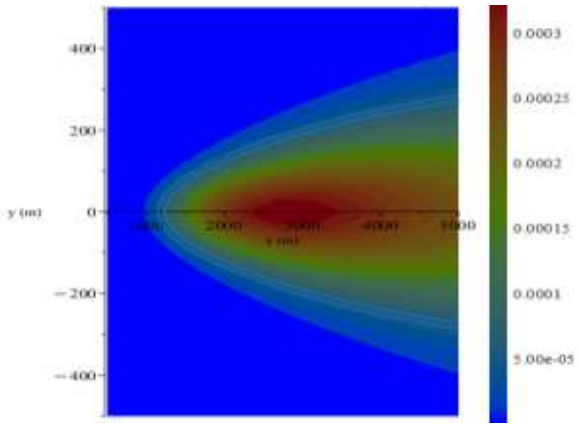

Fig. 4: 2D Contour Plot of the Ground-Level Concentration.

The 2D contour plot at ground level (Figure 4) provides a horizontal map view of the CO_2 distribution across the (x, y) plane. The highest concentrations appear along the plume centreline at approximately 3000m downwind, indicated by the red zone in the plot. As distance increases in either the crosswind (y) or downwind (x) direction, concentrations reduce progressively (transitioning from red to green and then to blue). The symmetrical pattern across the centreline is consistent with Gaussian plume dispersion theory, with the rate of crosswind dilution being faster than the downwind reduction after the peak.

CONCLUSION

The findings from this research demonstrate that the dispersion of CO_2 from the Ibom Power Plant is quantitatively shaped by the interplay of emission parameters, atmospheric stability and dispersion coefficients. The localized Gaussian plume model developed in this study, which incorporates a first-order reaction term, successfully identifies a critical impact zone between 2000 m and 5000 m downwind where ground-level CO_2 concentrations are predicted to be highest, particularly under stable atmospheric conditions. The model's outputs, including the narrow, concentrated plume structure along the centreline and the vertical concentration profile peaking near the effective stack height, are consistent with the theoretical behavior of elevated point sources.

REFERENCES

Awodumi, O. B. & Adewuyi, A. O. (2020). The role of non-renewable energy consumption in economic growth and carbon emission: Evidence from oil producing economies in Africa. *Energy Strategy Reviews*, Volume 27, 100434, ISSN 2211-467X. https://doi.org/10.1016/j.esr.2019.100434

Cioclea, D., Radu, S.M., Cămărășescu, A., Matei, A. & Drăgoescu, R. (2024). CFD Simulation of Carbon Dioxide Dispersion Dynamics in Closed Spaces. *Mining Revue*, 30(1), 2024. 72-77. https://doi.org/10.2478/minrv-2024-0008

IEA. (2019). Africa Energy Outlook 2019. Retrieved from https://www.iea.org/reports/africa-energy-outlook-2019

IEA. (2020). Energy Technology Perspectives 2020 - Special Report on Carbon Capture Utilisation and Storage: CCUS in clean energy transitions, OECD Publishing, Paris, https://doi.org/10.1787/208b66f4-en

IEA. (2022). Global Energy Review: CO2 Emissions in 2021, IEA, Paris. Retrieved from https://www.iea.org/reports/global-energy-review-co2-emissions-in-2021-2

IEA. (2023). CO_2 emissions in 2022. Retrieved from https://www.iea.org/reports/co2-emissions-in-2022.0

Intergovernmental Panel on Climate Change (IPCC) (2021). Climate Change 2021: The Physical Science Basis. IPCC Sixth Assessment Report. Retrieved from https://www.ipcc.ch/report/ar6/wg1/

Ogunjobi, J. O., Ogunjumo, R. A. & Ibitowa, S. A. (2024). Carbon Dioxide Emissions from Energy Consumption, Foreign Direct Investment and Economic Growth in Nigeria: A Multivariate Causal Analysis. *International Journal of Energy Economics and Policy*, 15(1), 513–518. https://doi.org/10.32479/ijeep.18118

Samborska-Goik, K. & Pogrzeba, M. (2024). A Critical Review of the Modelling Tools for the Reactive Transport of Organic Contaminants. *Applied Sciences*, 14(9), 3675. https://doi.org/10.3390/app14093675

Seinfeld, J.H. & Pandis, S.N. (2016). *Atmospheric Chemistry and Physics: From Air Pollution to Climate Change* (3rd Edition). Wiley, ISBN 978-1-118-94740-1. https://www.wiley.com/en-us/Atmospheric+Chemistry+and+Physics

Turner, D. B. (1994). *Workbook of atmospheric dispersion estimates: An introduction to dispersion modeling.* (2nd edition). CRC Press, Cincinnati.

United States Environmental Protection Agency (USEPA). (2025). Greenhouse gas emissions from a typical passenger vehicle. Retrieved from https://www.epa.gov/greenvehicles

Wang, H., Liu, B., Liu, X., Lü, C., Deng, J. & You, Z. (2021). Dispersion of carbon dioxide released from buried high-pressure pipeline over complex terrain. *Environmental Science and Pollution Research*, 28(6), 6635–6648. https://doi.org/10.1007/s11356-020-11012-7

Zhang, L., Liu, P., Zhao, L., Wang, G., Zhang, W. & Liu, J. (2021). Air quality predictions with a semi-supervised bidirectional LSTM neural network. *Atmospheric Pollution Research*, 12(1), 328–339. https://doi.org/10.1016/J.APR.2020.09.003